School of Natural Sciences and Mathematics

Superfluidity in the Absence of Kinetics in Spin-Orbit-Coupled Optical Lattices

UT Dallas Author(s):

Chuanwei Zhang

Citation:

Hui, Hoi-Yin, Yongping Zhang, Chuanwei Zhang, and V. W. Scarola. 2017. "Superfluidity in the absence of kinetics in spin-orbit-coupled optical lattices." Physical Review A 95(3): 033603: 1-7, doi:10.1103/PhysRevA.95.033603

Superfluidity in the absence of kinetics in spin-orbit-coupled optical lattices

Hoi-Yin Hui,[1] Yongping Zhang,[2] Chuanwei Zhang,[3] and V. W. Scarola[1]
[1]*Department of Physics, Virginia Tech, Blacksburg, Virginia 24061, USA*
[2]*Department of Physics, Shanghai University, 200444 Shanghai, China*
[3]*Department of Physics, The University of Texas at Dallas, Richardson, Texas 75080, USA*
(Received 8 July 2016; published 2 March 2017)

At low temperatures bosons typically condense to minimize their single-particle kinetic energy while interactions stabilize superfluidity. Optical lattices with artificial spin-orbit coupling challenge this paradigm, because here kinetic energy can be quenched in an extreme regime where the single-particle band flattens. To probe the fate of superfluidity in the absence of kinetics we construct and numerically solve interaction-only tight-binding models in flatbands. We find that superfluid states arise entirely from interactions operating in quenched kinetic energy bands, thus revealing a distinct and unexpected condensation mechanism. Our results have important implications for the identification of quantum condensed phases of ultracold bosons beyond conventional paradigms.

DOI: 10.1103/PhysRevA.95.033603

I. INTRODUCTION

Experiments with ultracold atoms in optical lattices have opened investigations of strongly correlated systems in extreme regimes, in particular, the extremes of the Fermi-Hubbard and the Bose-Hubbard models. In the latter case, a quantum phase transition has been observed [1–3], where the balance between interaction and single-particle kinetics can be tuned to destabilize the superfluid (SF) into a Mott-insulating (MI) state of localized bosons [4–6].

Recent theoretical studies have found Bose condensation even in lattice systems with quenched kinetics that go beyond simply raising optical lattice depth to decrease intersite tunneling (hopping). Interesting consequences of condensation in flatbands include SFs derived solely from the interaction [7–10]. However, their experimental implementation faces challenges. For example, some of the proposals require long-range hoppings with specific ratios, while some require spatially varying hopping strengths. These are difficult to accomplish with ordinary atoms or molecules in simple optical lattices.

Recently, special optical lattice geometries hosting flatbands have been proposed and in some cases realized (e.g., hexagonal [11,12] and excited bands of kagome lattices [8,13]). Synthetic spin-orbit coupling (SOC) [14–18] has also been found to lead to flatbands [7,9,19,20] on regular lattices with Zeeman fields. It is therefore appropriate to investigate the characteristics of superfluidity, if it exists at all, in such flatband systems.

Previous studies of superfluidity in flatbands assumed definite incommensurate filling ratios, which leads to the formation of a condensate. Interactions are then included at the mean-field level. In realistic experiments with trapping potentials, it is, however, more pertinent to ask whether superfluidity persists for a finite range of chemical potential, or else the system could phase-separate to regions of MIs with different particles per site at low hopping. Also, the nonperturbative nature of flatband systems makes theoretical analyses nontrivial. Understanding superfluidity in such limits requires unbiased methods, for example, exact diagonalization or a density matrix renormalization group (DMRG), to go beyond mean field to understand how (or if) superfluidity can actually occur.

In this paper, we show how to create flatbands using Rashba spin-orbit coupling in one and two dimensions. We model the band structure and construct a tight-binding model. With an s-wave interaction between bosons placed in the flatband, we find that even in the absence of kinetics they condense and form a SF. We compute the mean-field phase diagram and find competing MI and SF phases (in direct analogy to what one finds by placing interacting bosons in an ordinary optical lattice with kinetics). We also go beyond the mean field to probe the role of quantum fluctuations by using DMRG [21–23] to show that the SF survives quantum fluctuations. Our central finding is that the interactions themselves define an effective band structure in which bosons condense to reveal a type of SF derived entirely from interactions that is fundamentally different from SOC SFs that have been studied up to now (see, e.g., Refs. [24–31]). This type of interaction-only SF has distinctive excitations which can be used to discern it from ordinary SFs.

II. CONTINUUM MODEL

We consider a two-component spin-orbit-coupled Bose-Einstein condensate in a d-dimensional optical lattice, described by the Hamiltonian

$$\hat{H} = \int d\boldsymbol{r}\hat{b}^\dagger(\boldsymbol{r})H_0(\boldsymbol{r})\hat{b}(\boldsymbol{r}) + \frac{U_0}{2}\int d\boldsymbol{r}\sum_{\sigma\sigma'}\hat{b}^\dagger_\sigma(\boldsymbol{r})\hat{b}^\dagger_{\sigma'}(\boldsymbol{r})\hat{b}_{\sigma'}(\boldsymbol{r})\hat{b}_\sigma(\boldsymbol{r}), \quad (1)$$

$$H_0 = \frac{\hbar^2\boldsymbol{k}^2}{2m} + \frac{\hbar k_R}{m}\boldsymbol{\mathcal{F}}\cdot\boldsymbol{\sigma} + \Omega\sigma_z + V_{\rm lat}\sum_{i=1}^{d}\sin^2\frac{\pi\boldsymbol{r}\cdot\boldsymbol{e}_i}{a}, \quad (2)$$

with $\hat{b}^\dagger = (\hat{b}^\dagger_\uparrow, \hat{b}^\dagger_\downarrow)$, where $\hat{b}^\dagger_\sigma(\boldsymbol{r})$ creates a particle with spin $\sigma \in \{\uparrow, \downarrow\}$ at position $\boldsymbol{r}$ (with unit vectors $\boldsymbol{e}_i$ defining chain and square lattices for $d = 1$ and 2, respectively), and U_0 is the s-wave interaction strength. In the single-particle Hamiltonian H_0, m is the mass of each particle, $\boldsymbol{k}$ is the momentum operator,

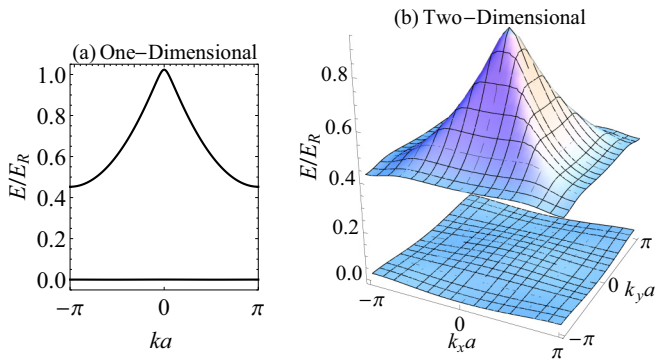

FIG. 1. Energy versus wave vector for the lowest two energy bands of Eq. (2) with $k_R = 2\pi/a$, $V_{\rm lat} = E_R$, for (a) the one-dimensional system, with $\Omega^* = 8.88E_R$, and (b) the two-dimensional system, with $\Omega^* = 8.31E_R$.

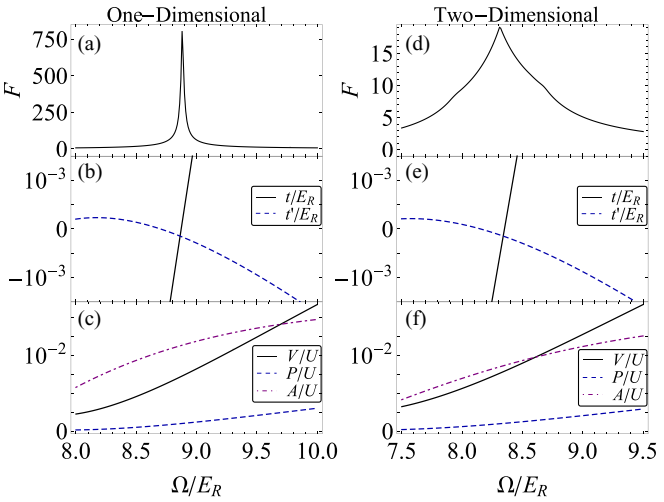

FIG. 2. (a) The flatness ratio (defined as the ratio of the gap between the two lowest bands to the width of the lowest band [9]) versus Rabi frequency for $k_R = 2\pi/a$ and $V_{\rm lat} = E_R$ in one dimension. (b) The hopping parameters t and t' against the Rabbi frequency. (c) The ratio of interaction parameters V, P, and A to U. The right column (d)–(f) plots the same quantities for a two-dimensional system (with the same k_R and $V_{\rm lat}$). Choosing Ω to lie at the peak leads to Eq. (3).

k_R characterizes the strength of the SOC induced by the Raman lasers, Ω is the Rabi frequency which acts as the Zeeman field, and $V_{\rm lat}$ is the depth of the optical lattice. In one dimension, $\boldsymbol{k} = \boldsymbol{\mathcal{F}} = -i\partial_x$ and $\boldsymbol{\sigma} = \sigma_x$, while in the two dimensions, $\boldsymbol{k} = (-i\partial_x, -i\partial_y)$, $\boldsymbol{\mathcal{F}} = (i\partial_y, -i\partial_x)$, and $\boldsymbol{\sigma} = (\sigma_x, \sigma_y)$, in which the Pauli matrices $\boldsymbol{\sigma}$ act on the spin sectors of $b^\dagger$. For convenience, we define the lattice recoil energy $E_R \equiv (\pi/a)^2\hbar^2/(2m)$ to express some of the parameters.

III. TIGHT-BINDING MODEL

We reduce the above continuum model to a tight-binding model and project the interactions to the flat Bloch band. In the absence of interaction, the Bloch functions $\psi_{\boldsymbol{k}}(\boldsymbol{r}) = u_{\boldsymbol{k}}(\boldsymbol{r})e^{i\boldsymbol{k}\cdot\boldsymbol{r}}$ are found by expanding $u_{\boldsymbol{k}}(\boldsymbol{r})$ in plane waves with periodicity commensurate with that of the lattice. For given k_R and $V_{\rm lat}$, an optimal value of Ω, Ω^* produces a lowest band with the highest flatness ratio [9]. Figure 1 shows the band structures in $d = 1$ and 2 where $\Omega = \Omega^*$, with $k_R = 2\pi/a$ and $V_{\rm lat} = E_R$. The dependence of F on Ω for the same parameters is plotted in Figs. 2(a) and 2(d), which shows that a high flatness ratio [the large peaks in Figs. 2(a) and 2(d)] is achievable with moderate parameter strengths.

We construct the Wannier functions to obtain the tight-binding model. We define a two-component Wannier function localized at cell $\boldsymbol{R}_i$, $w(\boldsymbol{r} - \boldsymbol{R}_i) = [w_\uparrow(\boldsymbol{r} - \boldsymbol{R}_i), w_\downarrow(\boldsymbol{r} - \boldsymbol{R}_i)]^T$, with $w_\sigma(\boldsymbol{r} - \boldsymbol{R}_i) = \sum_{\boldsymbol{k}} e^{i\boldsymbol{k}\cdot(\boldsymbol{r}-\boldsymbol{R}_i)}u_{\sigma\boldsymbol{k}}(\boldsymbol{r})$, where $u_{\sigma\boldsymbol{k}}(\boldsymbol{r})$ are the Bloch functions for the lowest band. The phases of the Bloch functions are fixed by requiring the spread of the Wannier function, $\langle \boldsymbol{r}^2\rangle - \langle \boldsymbol{r}\rangle^2$ (where $\langle \boldsymbol{r}^l\rangle \equiv \sum_{\sigma\boldsymbol{k}} \langle u_{\sigma\boldsymbol{k}}|(i\nabla_{\boldsymbol{k}})^l|u_{\sigma\boldsymbol{k}}\rangle$), to be minimized [32]. The tight-binding model is constructed by effecting the transformation to the flatband spinor basis states, $\hat{a}_i^\dagger = \Sigma_\sigma \int d\boldsymbol{r} w_\sigma(\boldsymbol{r} - \boldsymbol{R}_i)\hat{b}_\sigma^\dagger(\boldsymbol{r})$, onto Eq. (1), with which the tight-binding parameters can then be readily computed by taking the overlaps of $w(\boldsymbol{r})$ (see Appendix B).

The noninteracting part of the Hamiltonian leads to hopping terms $(-t\sum_{\langle ij\rangle}\hat{a}_i^\dagger\hat{a}_j + \text{H.c.}$, where $\langle ij\rangle$ denotes nearest neighbors, and $-t'\sum_{\langle\langle ij\rangle\rangle}\hat{a}_i^\dagger\hat{a}_j + \text{H.c.}$, where $\langle\langle ij\rangle\rangle$ denotes next-nearest neighbors) and the chemical potential term $(-\mu\sum_i \hat{a}_i^\dagger\hat{a}_i)$. For a range of parameter values, we have numerically computed t, t', and μ and verified that the band dispersion resulting from these terms agrees very well with the band structure obtained directly from the plane-wave expansion of Eq. (2) (to within 5%), indicating the adequacy of our tight-binding approximation. At $k_R = 2\pi/a$ and $V_{\rm lat} = E_R$, the values of t and t' are plotted against Ω in Figs. 2(b) and 2(e). At the optimal flatness point ($\Omega = \Omega^*$), t and t' are vanishingly small ($<10^{-4}E_R$, compared with $t = 0.178E_R$ at $\Omega = 0$) and are much smaller than the density-assisted hopping A. (For example, for ^{87}Rb atoms with $k_R = 2\pi/a$ in a lattice with $a = 384$ nm and $V_{\rm lat} = E_R$ [18], $t'/A \approx t/A \approx 0.075$ at the optimal point, where the density-assisted term proportional to A is defined in the next paragraph.) This motivates us to drop the hopping terms in the effective tight-binding model and investigate the resulting interacting flatband model.

When truncated to the nearest-neighbor terms, the interaction [U_0 in Eq. (1)] in general leads to four terms in the tight-binding model, which are the on-site interaction $(U/2)\sum_i \hat{n}_i(\hat{n}_i - 1)$ (where $\hat{n}_i = \hat{a}_i^\dagger\hat{a}_i$), nearest-neighbor interaction $V\sum_{\langle ij\rangle}\hat{n}_i\hat{n}_j$, density-assisted hopping $-A\sum_{\langle ij\rangle}[\hat{a}_j^\dagger(\hat{n}_i + \hat{n}_j)\hat{a}_i + \text{H.c.}]$, and pair hopping $P\sum_{\langle ij\rangle}(\hat{a}_i^\dagger\hat{a}_i^\dagger\hat{a}_j\hat{a}_j + \text{H.c.})$. Their dependencies on Ω for $k_R = 2\pi/a$ and $V_{\rm lat} = E_R$ are plotted in Figs. 2(c) and 2(f). It is important to stress that in a "trivially flat" band where hoppings (t and t') are suppressed by increasing the depth of the lattice, both A and V are also suppressed, making the system classical. In contrast, for the system we are investigating, only the hoppings are suppressed.

Since P is much smaller than V or A near Ω^*, we drop the pair-hopping term in the tight-binding model. We also note that near Ω^*, V and A have similar values. This leads us to

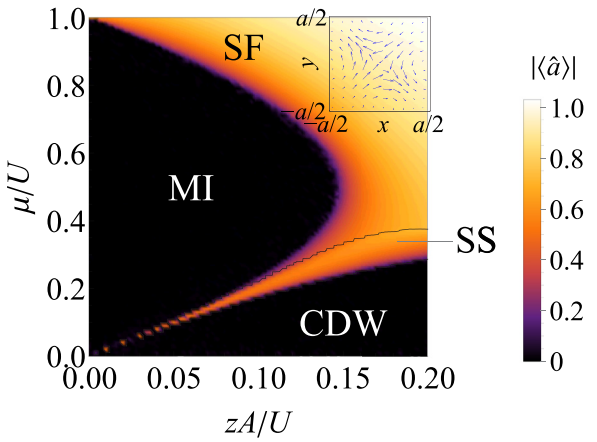

FIG. 3. The magnitude of the SF order parameter $|\langle\hat{a}\rangle|$ against μ and $A(=V)$ in the model Eq. (3). $z = 2\,(z = 4)$ is the coordination number in one (two) dimensions. The MI and CDW phases have $|\langle\hat{a}\rangle| = 0$ and the SF and SS phases have $|\langle\hat{a}\rangle| \neq 0$. The boundary between the SF and the SS phase is set at $\mathrm{var}\langle\hat{a}\rangle = 0.001$. The inset shows the superfluid spin texture (Appendix C) in a unit cell for the two-dimensional system in the superfluid phase at its optimal flatness point as in Fig. 1(b), leading to $V \approx A \approx 0.01U$.

study the interaction-only tight-binding model:

$$\hat{H}_{TB} = -\mu \sum_i \hat{n}_i + \frac{U}{2} \sum_i \hat{n}_i(\hat{n}_i - 1) + V \sum_{\langle ij\rangle} \hat{n}_i \hat{n}_j - A \sum_{\langle ij\rangle} [\hat{a}_j^\dagger(\hat{n}_i + \hat{n}_j)\hat{a}_i + \text{H.c.}], \quad (3)$$

where $V \approx A \approx 0.01U$ for the parameters we have chosen (see Fig. 3). V and A can be varied with V_{lat} and k_R, and the corresponding optimal value of Ω, in Eq. (2). For simplicity and in line with what we observe in Fig. 2, we set $A = V$ in the rest of our numerical study. We have checked that slight deviations from this condition do not qualitatively alter the phase diagrams presented.

IV. MEAN-FIELD PHASE DIAGRAM

We now turn to an analysis of the phases of Eq. (3). We first adopt a mean-field approach which ignores quantum fluctuations. Quantum fluctuations become more important in low dimensions. In the following section we shall examine the role of quantum fluctuations using DMRG in one dimension. We will show that the mean-field approach presented in this section gives qualitatively correct results.

We construct the mean-field phase diagram of Eq. (3) using the Gutzwiller ansatz wave function, $|\Psi\rangle = \prod_i \sum_n f_n^i |n\rangle_i$, where $|n\rangle_i$ is the Fock state with n bosons at the ith site [4,35]. We obtain the mean-field ground state by minimizing $\langle\Psi|\hat{H}_{TB}|\Psi\rangle$ with respect to f_n^i. To characterize the ground state, we compute the average SF order parameter $\langle\hat{a}\rangle$, its spatial variance $\mathrm{var}\langle\hat{a}\rangle$, and the spatial variance of the occupation number $\mathrm{var}\langle\hat{n}\rangle$. With these we can identify the MI phase (with $\langle\hat{a}\rangle = 0$ and $\mathrm{var}\langle\hat{n}\rangle = 0$), the charge density wave (CDW) phase (with $\langle\hat{a}\rangle = 0$ and $\mathrm{var}\langle\hat{n}\rangle \neq 0$), the supersolid (SS) phase (with $\langle\hat{a}\rangle \neq 0$ and $\mathrm{var}\langle\hat{a}\rangle \neq 0$), and the SF phase (with $\langle\hat{a}\rangle \neq 0$ and $\mathrm{var}\langle\hat{a}\rangle = 0$).

The resulting phase diagram is shown in Fig. 3, with MI, CDW, and SS phases at small A and SF at large A. Its resemblance to that of the conventional extended Bose-Hubbard model [22,33,34,36] can be understood in a mean-field decoupling of the density-assisted hopping term [proportional to A in Eq. (3)]:

$$\hat{a}_i^\dagger \hat{n}_i \hat{a}_j \to \langle\hat{n}\rangle \hat{a}_i^\dagger \hat{a}_j.$$

Here the density-assisted hopping plays the role of conventional hopping to yield an effective band structure (with an effective hopping of strength $\langle\hat{n}\rangle A$). The mean-field phase diagram indicates that bosons still condense and form a superfluid phase even in the absence of kinetics. After condensing into the band minimum of the effective band, the residual interactions support the formation of a superfluid.

There are similarities and differences between the superfluid discussed here and the superfluids typically discussed in the ordinary Bose-Hubbard model of optical lattices with SOC. The mean-field superfluid order parameter $\langle\hat{a}\rangle$ defines a spinor when decomposed in terms of the original spinful bosons since $\langle\hat{a}_i\rangle = \int d\boldsymbol{r}[w_\uparrow(\boldsymbol{r} - \boldsymbol{R}_i)\langle\hat{b}_\uparrow(\boldsymbol{r})\rangle + w_\downarrow(\boldsymbol{r} - \boldsymbol{R}_i)\langle\hat{b}_\downarrow(\boldsymbol{r})\rangle]$. The superfluid discussed here therefore has a canted spin structure, which is to be expected from SOC coupling. But there are fundamental differences. The strength of superfluidity is determined almost entirely from interactions (not a competition between kinetics and interactions). Furthermore, the condensation of bosons occurs in an effective band with a density-dependent strength. But most importantly, the excitations of the superfluid discussed here are multiparticle because they derive entirely from interactions. The observable consequences of the differences will be discussed in the summary. We now address the role of quantum fluctuations.

V. PHASES IN LOW DIMENSIONS

To address the impact of quantum fluctuations on our phase diagram, we pass to a regime where quantum fluctuations are strongest: one dimension. Here we can use the DMRG method to compute what is essentially the exact phase diagram [22] so as to complement our mean-field results above. We will show qualitative agreement between our mean-field results for higher dimensions and our one-dimensional DMRG results. This shows that quantum fluctuations do not qualitatively change the conclusions drawn above.

To find the phase boundaries, we compute the ground-state energy of the model on a chain of length L with integer filling $E_L^{(0)}$ and compare this with the ground-state energies with $L \pm 1$ particles, $E_L^{(\pm)}$. The upper and lower chemical potential boundaries ($\mu_\pm$) of the gapped phase are $\mu_{\pm} = \lim_{L\to\infty}[E_L^{(\pm)}_{(0)} - E_L^{(0)}_{(-)}]$, where the limits are numerically computed by extrapolation from finite-L results. The upper boundary for the $\nu = 1$ Mott lobe obtained from this approach are plotted in Fig. 4(a). Here we see MI and superfluid phases expected from the mean-field theory. Quantum fluctuations force the otherwise rounded MI lobe to instead converge to a Berezinskii-Kosterlitz-Thouless point at the tip of the lobe [37].

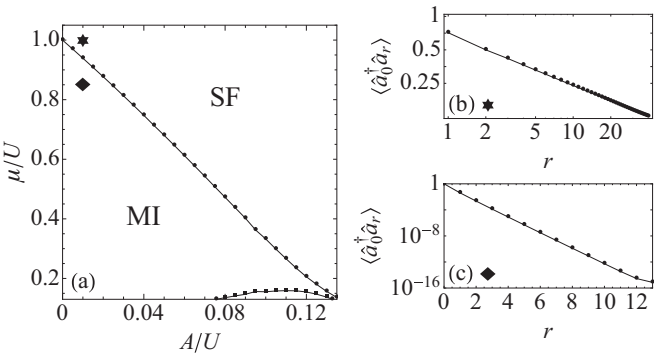

FIG. 4. (a) The gapped phase (MI with 1 particle per site) boundary defined by plotting the chemical potential against $A(=V)$ for Eq. (3). (b) The single-particle density matrix $\langle \hat{a}_0^\dagger \hat{a}_r \rangle$ versus distance r in the compressible phase [star in (a), with $\mu = U$ and $A = V = 0.01U$] on a log-log scale. (c) The same as (b) but in the gapped phase [diamond in (a), with $\mu = U$ and $A = V = 0.01U$] in the log-linear scale. The lines are a guide to the eye. Note that the chosen values of A in (b) and (c) are consistent with the estimated values for ^{87}Rb.

For an unambiguous identification of the gapped and the compressible phases, we also compute the off-diagonal order (ODO), $\langle \hat{a}_0^\dagger \hat{a}_r \rangle$, for representative points in the two phases. Figure 4(b) plots the ODO against distance r for the compressible phase in a log-log scale. Since the data falls roughly on a straight line, it shows that the ODO decays algebraically, which is indicative of a superfluid phase in one dimension. In contrast, the ODO decays exponentially in the gapped phase [log-linear plot of Fig. 4(c)]. Superfluidity is absent there and the phase is a MI.

Our results show qualitative agreement between the mean-field phase diagram (Fig. 3) and the DMRG results in (Fig. 4). The presence of a superfluid phase in both phase diagrams shows that quantum fluctuations should preserve the MI and superfluid even in two dimensions, since quantum fluctuations are less severe in two dimensions.

VI. DISCUSSION

The parameter regime discussed here is accessible with current setups. For example, a recent experiment [38] with ^{87}Rb implemented spin-orbit coupling strengths and optical lattice depths ($k_R = 1.96\pi/a$ and $V_{\rm lat} = 1.4E_R$, respectively) in one dimension, near the regime considered here ($k_R = 2\pi/a$ and $V_{\rm lat} = 1E_R$). Another experiment [18] implemented SOC in two dimensions with ^{87}Rb atoms. Using the experimental values of $a = 384$ nm and assuming the perpendicular confinement of strength $V_{{\rm lat},\perp} = 81E_R$, we find $t \approx 2$ Hz, $A \approx 27$ Hz, and $U \approx 3$ kHz. These realistic parameters lead to a ratio $A \approx V \approx 0.01U$, which is strong enough to reveal the MI-superfluid transition. Figures 4(b) and 4(c) demonstrate the superfluid and Mott phases realized under these values.

The superfluid phase discussed here has unique experimental identifiers that contrast from the conventional superfluid states observed in optical lattice experiments [6]. We first note that here the superfluid-MI transition occurs at a very low lattice depth, $V_{\rm lat} \approx 1E_R$. Furthermore, the superfluid-MI phase boundaries are defined by the interaction strength, which depends on the lattice depth only insofar as the Wannier functions modify the s-wave scattering contribution to U and A. Second, we point out that since the physics discussed here is driven by density-assisted tunneling, methods to observe density-assisted tunneling [39] could be implemented to prove the dominance of this process. But the most important distinction stems from the unique nature of the interaction-only superfluid itself. Here the excitations must occur in the two-particle sector, since they derive entirely from two-particle interactions. As such, probes of excitations should have unique signatures. For example, the momentum distribution peaks in superfluid phases [6] show additional structure due to particle-hole excitations—the visibility (defined as $\frac{n_{\rm max}-n_{\rm min}}{n_{\rm max}+n_{\rm min}}$, where $n_{\rm max/min}$ are the maximum and minimum intensity along the circle $|k| = k_R$ in the momentum distribution [40,41]), scales linearly with the density $\approx(\langle \hat{n} \rangle + 1)4zt/3U$, where z is the coordination for ordinary superfluid [40,41]. On the other hand, since the superfluid discussed here is derived solely from the interaction ($A\hat{a}_j^\dagger \hat{n}_i \hat{a}_i$), its visibility should scale with the *square* of the density $\approx(\langle \hat{n} \rangle + 1)\langle \hat{n} \rangle 4zA/3U$. (The position of the peaks should be the same as that of ordinary superfluid, provided that the density is uniform.) Other more local probes are also possible. The realistic parameters we have ($t/U < 0.001$) would normally result in a Mott state at the trap center if the assisted tunneling term (A) were absent. But the observation of a finite condensate fraction near the trap center would yield strong evidence for the superfluid discussed here. Another, more direct example would employ atomic gas microscopes. These setups [42–45] offer direct probes of the dynamics under the effective Hamiltonian and would reveal the unique two-particle nature of the excitations.

It is widely understood that bosons condense into the lowest single-particle kinetic energy state while interactions perturb Bose-Einstein condensates into a superfluid state. We have studied optical lattice bosons in a flat spin-orbit band generated by Rashba spin-orbit coupling. We have derived and solved an interaction-only tight-binding model to show that even in the absence of kinetics the interaction itself leads to an effective band that allows condensation and the formation of a superfluid.

ACKNOWLEDGMENTS

V.W.S. and H.H. acknowledge support from AFOSR (FA9550-15-1-0445) and ARO (W911NF-16-1-0182). C.Z. is supported by ARO (W911NF-12-1-0334) and the NSF (PHY-1505496).

APPENDIX A: MAXIMALLY LOCALIZED WANNIER FUNCTIONS

We briefly review the computational procedure for obtaining the maximally localized wave function for the lowest band. We follow closely the treatment of Ref. [32] for isolated bands on a square lattice.

By using Bloch's theorem, the single-particle wave function in the lattice can be written as $\psi_{\sigma \boldsymbol{k}}(\boldsymbol{r}) = \sum_{\boldsymbol{K}} c_{\sigma,\boldsymbol{k}-\boldsymbol{K}} e^{i(\boldsymbol{k}-\boldsymbol{K})\cdot\boldsymbol{r}}$, where $\boldsymbol{k}$ is the crystal momentum and $\boldsymbol{K}$ are the reciprocal lattice vectors. Substituting this form of $\psi_{\sigma \boldsymbol{k}}(\boldsymbol{r})$ into

$H_0\psi = \mathcal{E}\psi$ yields

$$\left\{\frac{\hbar^2}{2m}(\boldsymbol{k}-\boldsymbol{K})^2 + \frac{\hbar k_R}{m}[(k_x - K_x)\sigma_y - (k_y - K_y)\sigma_x] + \Omega\sigma_z\right\} \times c_{\boldsymbol{k}-\boldsymbol{K}} + \sum_{\boldsymbol{K}'} U_{\boldsymbol{K}'-\boldsymbol{K}} c_{\boldsymbol{k}-\boldsymbol{K}'} = \mathcal{E} c_{\boldsymbol{k}-\boldsymbol{K}}, \tag{A1}$$

where $c_{\boldsymbol{k}-\boldsymbol{K}} = (c_{\uparrow\boldsymbol{k}-\boldsymbol{K}}, c_{\downarrow\boldsymbol{k}-\boldsymbol{K}})^T$, and

$$U_{\boldsymbol{K}} = \frac{V_{\text{lat}}}{a^2}\int_0^a\int_0^a dxdy\left(\sin^2\frac{\pi x}{a} + \sin^2\frac{\pi y}{a}\right)e^{-i(K_x x - K_y y)}. \tag{A2}$$

For each value of $\boldsymbol{k}$, we solve the ground state to construct the wave function. To fix the phases of the Bloch wave functions, we now rewrite the wave function as $\psi_{\sigma\boldsymbol{k}}(\boldsymbol{r}) = e^{i\phi(\boldsymbol{k})}u_{\sigma\boldsymbol{k}}(\boldsymbol{r})e^{i\boldsymbol{k}\cdot\boldsymbol{r}}$, where $u_{\sigma\boldsymbol{k}}(\boldsymbol{r}) = \sum_{\boldsymbol{K}} c_{\sigma,\boldsymbol{k}-\boldsymbol{K}} e^{-i\boldsymbol{K}\cdot\boldsymbol{r}}$ and the phases $\phi(\boldsymbol{k})$ are to be fixed. Following Ref. [32] we define

$$\tilde{M}^{(\boldsymbol{k},\boldsymbol{b})} = e^{-i\phi(\boldsymbol{k})+i\phi(\boldsymbol{k}+\boldsymbol{b})}\langle u_{\boldsymbol{k}}|u_{\boldsymbol{k}+\boldsymbol{b}}\rangle \tag{A3}$$

$$\equiv e^{-i\phi(\boldsymbol{k})+i\phi(\boldsymbol{k}+\boldsymbol{b})}M^{(\boldsymbol{k},\boldsymbol{b})}, \tag{A4}$$

where the inner product is defined as the summation over the spin index followed by an integral over a unit cell, and $u_{\boldsymbol{k}+\boldsymbol{b}}$ is normalized such that $\langle u_{\boldsymbol{k}}|u_{\boldsymbol{k}+\boldsymbol{b}}\rangle = 1$. The vectors $\boldsymbol{b}$ point to the four nearest neighbors (or two in one dimension) in the discretization of the Brillouin zone.

The phases are fixed by requiring $G^{(\boldsymbol{k})} = \sum_{\boldsymbol{b}} \text{Im}\ln\tilde{M}^{(\boldsymbol{k},\boldsymbol{b})}$ to vanish identically for all $\boldsymbol{k}$ [32]. Written in terms of $\phi(\boldsymbol{k})$ and $M^{(\boldsymbol{k},\boldsymbol{b})}$, we have

$$\sum_{\boldsymbol{b}}[\phi(\boldsymbol{k}+\boldsymbol{b}) - \phi(\boldsymbol{k})] = \sum_{\boldsymbol{b}}\text{Im}\ln M^{(\boldsymbol{k},\boldsymbol{b})}, \tag{A5}$$

which is recognized as a (discretized) Poisson equation for the phase field $\phi(\boldsymbol{k})$, and is amenable to standard numerical treatments.

APPENDIX B: TIGHT-BINDING PARAMETERS

By substituting the transformation

$$\hat{b}_\sigma(\boldsymbol{r}) = \sum_i w_\sigma(\boldsymbol{r} - \boldsymbol{R}_i)\hat{a}_i \tag{B1}$$

into $\hat{H}$ and ignoring integrals involving Wannier functions with more than two lattice sites apart, the Hamiltonian becomes

$$\hat{H} \approx -t\sum_{\langle ij\rangle}\hat{a}_i^\dagger\hat{a}_j - t'\sum_{\langle\langle ij\rangle\rangle}\hat{a}_i^\dagger\hat{a}_j + \text{H.c.} - \mu\sum_i\hat{a}_i^\dagger\hat{a}_i + \frac{U}{2}\sum_i\hat{n}_i(\hat{n}_i - 1) + V\sum_{\langle ij\rangle}\hat{n}_i\hat{n}_j - A\sum_{\langle ij\rangle}[\hat{a}_j^\dagger(\hat{n}_i + \hat{n}_j)\hat{a}_i + \text{H.c.}] + P\sum_{\langle ij\rangle}(\hat{a}_i^\dagger\hat{a}_i^\dagger\hat{a}_j\hat{a}_j + \text{H.c.}) \tag{B2}$$

with tight-binding parameters

$$\mu = -\int d\boldsymbol{r}\, w^\dagger(\boldsymbol{r})H_0 w(\boldsymbol{r}),$$

$$t = -\int d\boldsymbol{r}\, w^\dagger(\boldsymbol{r})H_0 w(\boldsymbol{r} - \boldsymbol{r}_1),$$

$$t' = -\int d\boldsymbol{r}\, w^\dagger(\boldsymbol{r})H_0 w(\boldsymbol{r} - \boldsymbol{r}_2),$$

$$U = U_0\int d\boldsymbol{r}\sum_{\sigma\sigma'} w_\sigma^*(\boldsymbol{r})w_{\sigma'}^*(\boldsymbol{r})w_{\sigma'}(\boldsymbol{r})w_\sigma(\boldsymbol{r}),$$

$$V = 2U_0\int d\boldsymbol{r}\sum_{\sigma\sigma'} w_\sigma^*(\boldsymbol{r})w_{\sigma'}^*(\boldsymbol{r} - \boldsymbol{r}_1)w_{\sigma'}(\boldsymbol{r} - \boldsymbol{r}_1)w_\sigma(\boldsymbol{r}),$$

$$A = -U_0\int d\boldsymbol{r}\sum_{\sigma\sigma'} w_\sigma^*(\boldsymbol{r})w_{\sigma'}^*(\boldsymbol{r})w_{\sigma'}(\boldsymbol{r})w_\sigma(\boldsymbol{r} - \boldsymbol{r}_1),$$

$$P = \frac{U_0}{2}\int d\boldsymbol{r}\sum_{\sigma\sigma'} w_\sigma^*(\boldsymbol{r})w_{\sigma'}^*(\boldsymbol{r})w_{\sigma'}(\boldsymbol{r} - \boldsymbol{r}_1)w_\sigma(\boldsymbol{r} - \boldsymbol{r}_1),$$

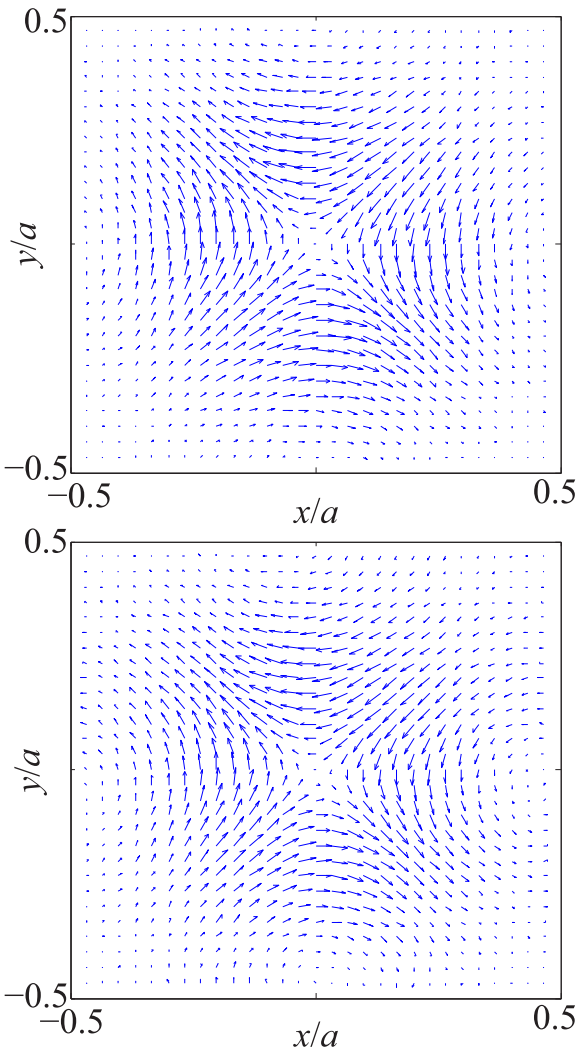

FIG. 5. The spin textures [Eqs. (C2)] for the Mott state (upper panel) and for the superfluid state (lower panel) in one unit cell at the same parameters as in Fig. 2 in the main text.

where $\boldsymbol{r}_1 = a\hat{e}_x$ and $\boldsymbol{r}_2 = \{^{2a\hat{e}_x,}_{a\hat{e}_x + a\hat{e}_y,} \; ^{d=1}_{d=2}$. By computing the maximally localized Wannier functions we are therefore able to find all tight-binding parameters.

APPENDIX C: SPIN TEXTURES

To compute the spin texture $\langle \hat{b}^\dagger \vec{\sigma} \hat{b} \rangle$ for the ground state, we use Eq. (B1) to express the $\hat{b}$ operators in terms of the $\hat{a}$ operators. We then apply the mean-field decoupling for both the Mott and superfluid phases. In the Mott state we have

$$\langle \hat{b}^\dagger_\alpha(\boldsymbol{r}) \hat{b}_\beta(\boldsymbol{r}) \rangle = \sum_{i,j} w^*_\alpha(\boldsymbol{r} - \boldsymbol{R}_i) w_\beta(\boldsymbol{r} - \boldsymbol{R}_j) \langle \hat{a}^\dagger_i \hat{a}_j \rangle = \sum_{i,j} w^*_\alpha(\boldsymbol{r} - \boldsymbol{R}_i) w_\beta(\boldsymbol{r} - \boldsymbol{R}_j) \delta_{ij} = \sum_i w^*_\alpha(\boldsymbol{r} - \boldsymbol{R}_i) w_\beta(\boldsymbol{r} - \boldsymbol{R}_i). \tag{C1}$$

On the other hand, in the superfluid phase we have

$$\langle \hat{b}^\dagger_\alpha(\boldsymbol{r}) \hat{b}_\beta(\boldsymbol{r}) \rangle = \sum_{i,j} w^*_\alpha(\boldsymbol{r} - \boldsymbol{R}_i) w_\beta(\boldsymbol{r} - \boldsymbol{R}_j) |\langle \hat{a} \rangle|^2.$$

We define the spin texture as the projection of the spins onto the x-y plane, with the components

$$S_x(\boldsymbol{r}) = 2\mathrm{Re}\langle b^\dagger_\uparrow(\boldsymbol{r}) b_\downarrow(\boldsymbol{r}) \rangle, \tag{C2a}$$

$$S_y(\boldsymbol{r}) = 2\mathrm{Im}\langle b^\dagger_\uparrow(\boldsymbol{r}) b_\downarrow(\boldsymbol{r}) \rangle. \tag{C2b}$$

In Fig. 5, we plot the spin textures in the Mott and the superfluid states.

[1] P. Verkerk, B. Lounis, C. Salomon, C. Cohen-Tannoudji, J.-Y. Courtois, and G. Grynberg, Phys. Rev. Lett. **68**, 3861 (1992).
[2] P. S. Jessen, C. Gerz, P. D. Lett, W. D. Phillips, S. L. Rolston, R. J. C. Spreeuw, and C. I. Westbrook, Phys. Rev. Lett. **69**, 49 (1992).
[3] A. Hemmerich and T. W. Hansch, Phys. Rev. Lett. **70**, 410 (1993).
[4] D. Jaksch, C. Bruder, J. I. Cirac, C. W. Gardiner, and P. Zoller, Phys. Rev. Lett. **81**, 3108 (1998).
[5] M. Greiner, O. Mandel, T. Esslinger, T. Hansch, and I. Bloch, Nature (London) **415**, 39 (2002).
[6] I. Bloch, J. Dalibard, and W. Zwerger, Rev. Mod. Phys. **80**, 885 (2008).
[7] S. D. Huber and E. Altman, Phys. Rev. B **82**, 184502 (2010).
[8] Y.-Z. You, Z. Chen, X.-Q. Sun, and H. Zhai, Phys. Rev. Lett. **109**, 265302 (2012).
[9] Y. Zhang and C. Zhang, Phys. Rev. A **87**, 023611 (2013).
[10] M. Tovmasyan, E. P. L. van Nieuwenburg, and S. D. Huber, Phys. Rev. B **88**, 220510 (2013).
[11] P. Soltan-Panahi, J. Struck, P. Hauke, A. Bick, W. Plenkers, G. Meineke, C. Becker, P. Windpassinger, M. Lewenstein, and K. Sengstock, Nat. Phys. **7**, 434 (2011).
[12] L. Tarruell, D. Greif, T. Uehlinger, G. Jotzu, and T. Esslinger, Nature (London) **483**, 302 (2012).
[13] G.-B. Jo, J. Guzman, C. K. Thomas, P. Hosur, A. Vishwanath, and D. M. Stamper-Kurn, Phys. Rev. Lett. **108**, 045305 (2012).
[14] J. Higbie and D. M. Stamper-Kurn, Phys. Rev. Lett. **88**, 090401 (2002).
[15] Y.-J. Lin, K. Jiménez-García, and I. B. Spielman, Nature (London) **471**, 83 (2011).
[16] V. Galitski and I. B. Spielman, Nature (London) **494**, 49 (2013).
[17] H. Zhai, Rep. Prog. Phys. **78**, 026001 (2015).
[18] Z. Wu, L. Zhang, W. Sun, X.-T. Xu, B.-Z. Wang, S.-C. Ji, Y. Deng, S. Chen, X.-J. Liu, and J.-W. Pan, Science **354**, 83 (2016).
[19] S. A. Parameswaran, I. Kimchi, A. M. Turner, D. M. Stamper-Kurn, and A. Vishwanath, Phys. Rev. Lett. **110**, 125301 (2013).
[20] F. Lin, C. Zhang, and V. W. Scarola, Phys. Rev. Lett. **112**, 110404 (2014).
[21] S. R. White, Phys. Rev. Lett. **69**, 2863 (1992).
[22] T. D. Kuhner, S. R. White, and H. Monien, Phys. Rev. B **61**, 12474 (2000).
[23] B. Bauer *et al.*, J. Stat. Mech: Theory Exp. (2011) P05001.
[24] M. Gong, Y. Qian, M. Yan, V. W. Scarola, and C. Zhang, Sci. Rep. **5**, 10050 (2015).
[25] H. Hu, B. Ramachandhran, H. Pu, and X.-J. Liu, Phys. Rev. Lett. **108**, 010402 (2012).
[26] Y. Qian, M. Gong, V. W. Scarola, and C. Zhang, arXiv:1312.4011.
[27] B. Ramachandhran, B. Opanchuk, X.-J. Liu, H. Pu, P. D. Drummond, and H. Hu, Phys. Rev. A **85**, 023606 (2012).
[28] B. Ramachandhran, H. Hu, and H. Pu, Phys. Rev. A **87**, 033627 (2013).
[29] J. D. Sau, R. Sensarma, S. Powell, I. B. Spielman, and S. Das Sarma, Phys. Rev. B **83**, 140510 (2011).
[30] C. Wu, I. Mondragon-Shem, and X.-F. Zhou, Chin. Phys. Lett. **28**, 097102 (2011).
[31] X. Zhou, Y. Li, Z. Cai, and C. Wu, J. Phys. B **46**, 134001 (2013).
[32] N. Marzari and D. Vanderbilt, Phys. Rev. B **56**, 12847 (1997).
[33] G. G. Batrouni, R. T. Scalettar, G. T. Zimanyi, and A. P. Kampf, Phys. Rev. Lett. **74**, 2527 (1995).
[34] A. van Otterlo, K. H. Wagenblast, R. Baltin, C. Bruder, R. Fazio, and G. Schon, Phys. Rev. B **52**, 16176 (1995).
[35] D. S. Rokhsar and B. G. Kotliar, Phys. Rev. B **44**, 10328 (1991).

[36] M. P. A. Fisher and L. I. Glazman, Proc. NATO Adv. Study Inst. **345**, 331 (1997).
[37] T. D. Kuhner and H. Monien, Phys. Rev. B **58**, R14741 (1998).
[38] C. Hamner, Y. Zhang, M. A. Khamehchi, M. J. Davis, and P. Engels, Phys. Rev. Lett. **114**, 070401 (2015).
[39] S. Baier, M. J. Mark, D. Petter, K. Aikawa, L. Chomaz, Z. Cai, M. Baranov, P. Zoller, and F. Ferlaino, Science **352**, 201 (2016).
[40] F. Gerbier, A. Widera, S. Fölling, O. Mandel, T. Gericke, and I. Bloch, Phys. Rev. Lett. **95**, 050404 (2005).
[41] F. Gerbier, A. Widera, S. Folling, O. Mandel, T. Gericke, and I. Bloch, Phys. Rev. A **72**, 053606 (2005).
[42] W. S. Bakr, J. I. Gillen, A. Peng, S. Fölling, and M. Greiner, Nature (London) **462**, 74 (2009).
[43] C. Weitenberg, M. Endres, J. F. Sherson, M. Cheneau, P. Schau, T. Fukuhara, I. Bloch, and S. Kuhr, Nature (London) **471**, 319 (2011).
[44] M. Miranda, R. Inoue, Y. Okuyama, A. Nakamoto, and M. Kozuma, Phys. Rev. A **91**, 063414 (2015).
[45] L. W. Cheuk, A. T. Sommer, Z. Hadzibabic, T. Yefsah, W. S. Bakr, and M. W. Zwierlein, Phys. Rev. Lett. **109**, 095302 (2012).